[2]Bazhenova, T. V., Gvozdeva, L. G., and Lobastov, Yu. G., *Shock Waves in Real Gases*, Nauka, Moscow, Russia, 1968 (in Russian).

[3]Slack, M. W., "Kinetics and Thermodynamics of the CN Molecule. 3. Shock Tube Measurements of CN Dissociation Rates," *Journal of Chemical Physics*, Vol. 64, No. 1, 1976, pp. 228–236.

[4]Park, C., Howe, J. T., Jaffe, R. L., and Candler, G., "Review of Chemical-Kinetic Problems of Future NASA Missions, II: Mars Entries," *Journal of Thermophysics and Heat Transfer*, Vol. 8, No. 1, 1994, pp. 9–23.

[5]Sturtevant, B., and Slachmuylders, E., "End Wall Heat-Transfer Effects on the Trajectory of a Reflected Shock Wave," *Physics of Fluids*, Vol. 7, No. 8, 1964, pp. 1201–1207.

[6]Goldsworthy, F. A., "The Structure of a Contact Region, with Application to the Reflection of a Shock from a Heat-Conducting Wall," *Journal of Fluid Mechanics*, Vol. 5, Pt. 1, 1959, pp. 164–176.

[7]Johannesen, N. H., Bird, G. A., and Zienkiewicz, H. K., "Theoretical and Experimental Investigations of the Reflexion of Normal Shock Waves with Vibrational Relaxation," *Journal of Fluid Mechanics*, Vol. 30, Pt. 1, 1967, pp. 51–64.

[8]Hanson, R. K., Presley, L. L., and Williams, E. V., "Numerical Solutions of Several Reflected Shock-Wave Flow Fields with Nonequilibrium Chemical Reactions," NASA TN D-6585, 1972.

[9]Provotorov, V. P., and Riabov, V. V., "Nonsteady-State Heat Transfer upon Shock Wave Reflection in a Shock Tube," *Journal of Applied Mechanics and Technical Physics*, Vol. 28, No. 5, 1987, pp. 721–727.

[10]Ermakov, V. V., and Kalitkin, N. N., "The Optimal Step in Newton's Regularization Method," *Journal of Computational Mathematics and Mathematical Physics*, Vol. 21, No. 2, 1981, pp. 235–242.

[11]Denisenko, O. V., and Provotorov, V. P., "Study of Viscous Gas Flows in Multicomponent Mixtures," *Trudy TsAGI*, Issue 2269, 1985 (in Russian).

[12]Provotorov, V. P., "Improved Regularization Algorithm for Computation of the Thin-Viscous-Shock-Layer Equations," *Trudy TsAGI*, Issue 2436, 1990, pp. 165–173 (in Russian).

Charge Optimization for a Triangular-Shaped Etched Micro Heat Pipe

A. B. Duncan*
University of Illinois at Chicago, Chicago, Illinois 60607
and
G. P. Peterson†
Texas A&M University, College Station, Texas 77843

Nomenclature

$R_{c,e}$ = liquid/vapor interface radius of curvature, evaporator
$R_{\max}$ = liquid/vapor interface radius of curvature, condenser
γ = liquid surface tension
ΔP_c = available capillary pressure difference
$\Delta P_{c,c}$ = condenser capillary pressure difference
$\Delta P_{c,e}$ = evaporator capillary pressure difference

Received Feb. 14, 1994; revision received Aug. 1, 1994; accepted for publication Sept. 27, 1994.

*Assistant Professor, Department of Mechanical Engineering. Member AIAA.

†Tenneco Professor and Head, Department of Mechanical Engineering. Member AIAA.

Introduction

PREVIOUS investigations have indicated that the primary transport limit occurring in micro heat pipes is the capillary pumping limit.[1] This limit occurs when the available capillary pressure difference between the evaporator and the condenser regions is not sufficient to overcome the liquid and vapor pressure drops. When the operating conditions of the heat pipe are such that the summation of the pressure losses associated with heat pipe operation exceed the available capillary pressure difference, the working fluid of the heat pipe will not be "pumped" from the condenser to the evaporator and the wicking structure will dry out. At high heat flux values, a condition may be reached where such a small amount of liquid exists in the evaporator that viscous forces in the liquid flow channel become larger than the capillary pressure difference and prohibit liquid from returning to the evaporator region. This phenomena of dryout defines the capillary wicking limit and is typically observed experimentally by either a sudden increase in evaporator temperature or a distinct decrease in effective thermal conductivity, as power input to the evaporator is increased.

Available Capillary Pressure Difference

The equation of Young and Laplace may be used to define the pressure difference between liquid and vapor phases at an arbitrarily curved interface. In order to apply this equation to the evaporator and condenser regions of a heat pipe, it must be assumed that during steady-state operation, the liquid-vapor interfaces are in a state of equilibrium with respect to the radius of curvature. It must also be assumed that mass depletion from the liquid phase in the evaporator and mass injection into the liquid phase in the condenser do not affect this equilibrium state. Historically, the equation of Young and Laplace has been used to evaluate the difference in capillary pressure between the evaporator and condenser regions in order to determine the available capillary pumping pressure for heat pipe operation as

$$\Delta P_c = \Delta P_{c,e} - \Delta P_{c,c} \tag{1}$$

When a heat pipe of triangular cross section is properly charged, a flooded condition will exist in the condenser region and the liquid-vapor interface in the condenser region will assume the shape of a hemisphere. Using a minimization of free surface energy technique,[2] the radius of curvature in this region can be shown to be equal to the largest radius of curvature that exists in the triangular cross section of the micro heat pipe (i.e., an inscribed circle), as illustrated in Fig. 1. For the etched micro heat pipes evaluated and tested in the current investigation, this radius of curvature $R_{c,e}$ is equal to 30.96 μm, and the equation of Young and Laplace reduces to[3]

$$\Delta P_{c,c} = 2\gamma/R_{\max} = 2\gamma/30.96\ \mu\text{m} \tag{2}$$

In the evaporator region, the liquid-vapor interface is initially assumed to be one dimensional (i.e., having only one nonzero radius of curvature). This assumes first, no axial variation in the radius of curvature in the evaporator, and second, that the cross-sectional radius of curvature is the same

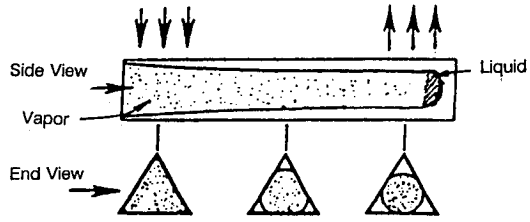

Fig. 1 Cross section of the micro heat pipe.

for each of the three corners at any steady-state operating condition (i.e., the gravitational body forces are neglected). It was also assumed that the working fluid, methanol, completely wet the silicon surface, implying that the apparent liquid-solid contact angle α was equal to zero. With these assumptions, defining the radius of curvature of the liquid-vapor interface in the evaporator defined the entire liquid configuration in the evaporator.

To determine the maximum heat transport capacity of the micro heat pipes, the radius of curvature of the liquid-vapor interface in the evaporator was varied and the available capillary pressure of the micro heat pipe was calculated. This available capillary pressure was then compared with the corresponding of the pressure drops associated with the flow of the liquid and vapor phases.

The pressure drop associated with the flow of the liquid phase was calculated utilizing the analysis of Chi.[4] Based on the conclusions of Ivanovskii et al.[5] and Bankston and Smith,[6] the pressure drop associated with flow of the vapor phase was calculated using a Poiseuille flow analysis. The hydrostatic pressure drop associated with the horizontally oriented micro heat pipes of the current investigation was calculated as the product of the working fluid liquid density, the acceleration due to gravity, and the hydraulic radius of the triangular cross section.

As mentioned previously, the liquid/vapor interface was assumed to exist with constant radii of curvature in both the evaporator and condenser regions. The radius of curvature of the liquid/vapor interface in the adiabatic region of the micro heat pipe was assumed to increase linearly from that assumed in the evaporator region to that which occurred in the flooded condenser region, 30.96 μm. In this manner the flow areas of both the liquid and vapor phases were defined. In order to accurately predict the pressure drop terms associated with the flow of the liquid and vapor phases, the adiabatic region was divided into a number of finite volumes, and the sum of the pressure drops associated with each of these regions was used to approximate the total pressure drop in the adiabatic section of the micro heat pipe. Each of the finite volumes utilized liquid and vapor phase flow areas that were representative of the actual flow area based on the assumed linear distribution of the radius of curvature of the liquid/vapor interface. The computer model used to investigate the capillary limit of the etched micro heat pipes determined the physical properties of the working fluid based on a single operating temperature. This operating temperature is typically representative of the temperature in the adiabatic region of the micro heat pipe. Initially, an investigation was conducted to determine the optimal operating temperature using methanol as the working fluid. To do this both the radius of curvature of the liquid/vapor interface in the evaporator region and the operating temperature were varied. Through the analytical model, the optimal operating temperature of the micro heat pipe using methanol as a working fluid was calculated to be approximately 385 K, with a corresponding maximum heat transport capacity of 0.9 mW. This operating temperature was utilized in the subsequent portions of the analytical investigation to determine the maximum performance characteristics of the micro heat pipes.

Figure 2 illustrates the operating characteristics of the triangular etched micro heat pipe as predicted by the analytical model of the capillary limit. The solid line in Fig. 2 represents the available capillary pressure difference, predicted by varying the radius of curvature of the liquid/vapor interface in the evaporator region from zero to the maximum possible value in the condenser.

Region 1 of Fig. 2 represents the "nonoperational" liquid/vapor configurations for the micro heat pipe. In region 1, the total pressure drop, i.e., the sum of the hydrostatic pressure drop and the pressure drops associated with the flow of the liquid and vapor phases, corresponding to the three greatest input power levels (1.2, 0.9, and 0.5 mW) exceed the available capillary pressure difference. However, as the evaporator capillary radius increases, leading into region 3, only the greatest value of input power (1.2 mW) continues to produce a pressure drop in excess of the available capillary pressure difference of the micro heat pipe. This indicates that the input power of 1.2 mW exceeds the capillary limit of the micro heat pipe. The curve representing the total pressure drop associated with an input power of 0.9 mW intersects the curve representing the available capillary pressure difference at a point which corresponds to a radius of curvature in the evaporator region of approximately 13.7 μm. This, in effect, defines the entire configuration of the liquid in the micro heat pipe for that input power. For an input power of 0.5 mW the evaporator radius of curvature required for operation is approximately 20.5 μm and for 0.2 mW is approximately 22.5 μm.

Region 2 of Fig. 2 represents operating parameters for which the available capillary pressure difference exceeds the total pressure drop associated with the two lower input power values (0.2 and 0.5 mW). Note, however, that these two curves do again intersect the curve representing the available capillary pressure difference in this region. In other words, there are two possible configurations that satisfy the capillary pressure "balance" of the micro heat pipe. The slope of the curves representing total pressure drop in region 2 indicates, however, that the solutions in this region are unstable by nature, and implies that the system will seek the more stable configuration that corresponds to the greater radius of curvature in the evaporator region.

Using the information provided by the capillary limit analysis, the radius of curvature in the evaporator region of the micro heat pipe was calculated for all input power values less than the capillary limit. With the known radius of curvature in the evaporator, adiabatic, and condenser regions, the optimal liquid charge could be predicted as a function of input power. Figure 3 illustrates the resulting optimal liquid charge as a function of input power. As shown, this liquid charge

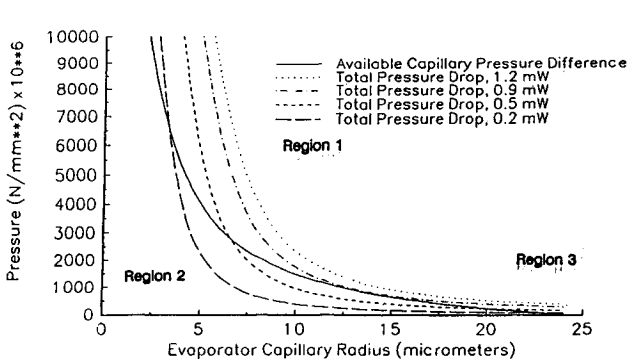

Fig. 2 Available capillary pressure and total pressure drop as a function of capillary radius.

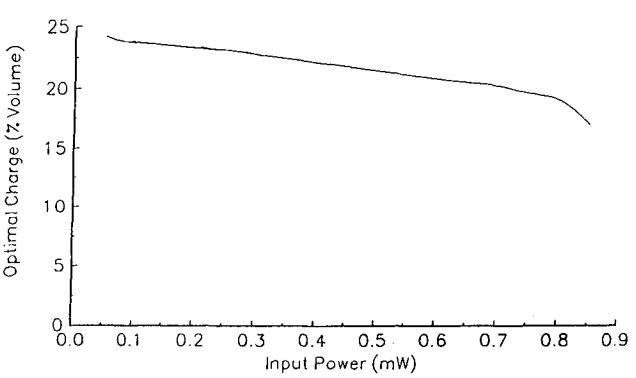

Fig. 3 Optimal liquid charge as a function of input power (T = 385 K).

Table 1 Measured heat transport at onset of dry out

% Liquid charge	Measured heat transport, mW
10	1.02
20	3.38
30	3.76
50	5.53

Input power = 2.00 W.
Predicted heat transport at onset of dryout = 0.9 mW.

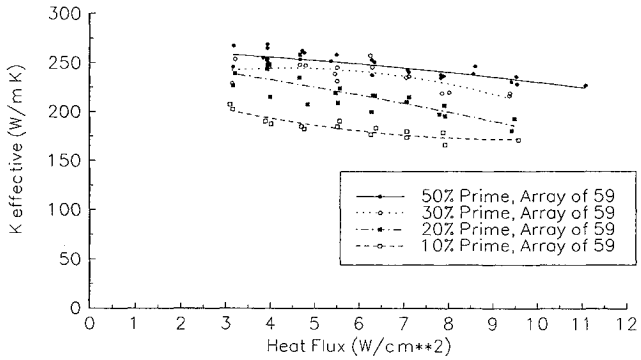

Fig. 4 Observed effective thermal conductivity of the micro heat pipe arrays.

varies from approximately 25% of the total micro heat pipe volume at input power values approaching zero to approximately 16% at the capillary limit of the micro heat pipe.

Comparison with Experimental Results

To validate this analysis, an experimental investigation, similar to one previously conducted by Peterson et al.,[7] was undertaken. An anisotropic etching process was used to produce a series of 59 parallel, triangular channels each 120 μm wide and 80 μm deep, in silicon wafers. Once fabricated, a clear Pyrex® cover plate was bonded to the top surface of each wafer using an uv bonding technique. These micro heat pipe arrays were then evacuated and charged with varying amounts of methanol and evaluated using an IR thermal imaging unit to measure the temperature gradients and maximum localized temperatures. From these data, an effective thermal conductivity could be computed.

Figure 4 illustrates the experimental results for the four different fluid charges evaluated, 50, 30, 20, and 10% charge by volume, respectively. For comparison, the measured thermal conductivity of the plain wafers are also shown as a function of heat flux. As illustrated, the experimental results consistently indicated the gradual onset of dryout (indicated by the slight decrease in effective thermal conductivity) over the entire range of input power levels utilized in this investigation.

Considering the silicon and micro heat pipes as parallel thermal resistances subjected to the input power from the distributed heat source, the heat transported by each micro heat pipe can be determined from the experimental results. A heat flux value of 3.15 W/cm^2, which corresponds to a total heat input of 2.0 W, was the smallest input power value utilized in the current investigation. If this input power is considered to be that which corresponds to the onset of dryout, then dry out actually occurred at input power levels that were four to six times those predicted by the analytical model as illustrated in Table 1.

The difference between the predicted and measured capillary limit in this investigation can be attributed to three primary factors. First, the thermal and spatial resolution characteristics of the thermal imaging system were not high enough to observe and indicate the precise location and power level at which dryout occurred. Although the system was capable of detecting the temperature gradients, which were used to calculate the effective thermal conductivity of the wafers, the system was not capable of producing spatial resolution on the scale of 1 μm or less, which would be required in order to observe the progressive dry out of an individual micro heat pipe. Second, the analysis used to develop the model of the capillary limit relied solely on the assumptions associated with the mass and momentum transport characteristics of bulk fluids. Previous investigations have shown that thin liquid films such as those which exist in the evaporator section of micro heat pipes have tremendously enhanced evaporative characteristics when compared to the evaporative characteristics of bulk fluids. Finally, the analytical model does not account for the actual process of gradual dryout, wherein the wetted liquid front progresses toward the condenser allowing heat pipe operation to continue, though decreasing the effective heat pipe length. One other factor may provide a partial explanation for this difference, and this has to do with the initial charge. Excess liquid in the system would tend to move the actual point of dryout closer to the evaporator region of the heat pipe. This would, in effect, allow partial operation of the heat pipe to occur, increasing the effective thermal conductivity of the wafer/heat pipe array composite. For this reason, identification of the precise dryout heat flux and location will require a significantly different experimental approach.[8]

Conclusions

An analytical model has been developed for a triangular-shaped, etched micro heat pipe. This is the first analytical micro heat pipe model to predict not only the capillary limit of operation, but also the radius of curvature in the evaporator section and the optimal value of liquid charge. The model predicted optimal liquid prime values between 16–25% for various power levels, and indicated that the optimal charge value would not exceed 25%, even for input power levels near zero. The experimental investigation utilized micro heat pipe arrays that had liquid charge values ranging from 10 to 50%, and indicated that the effective thermal conductivity of the heat pipes continued to increase with increasing liquid charge.

To validate the analytical model, the predicted values of maximum heat transport capacity were compared with experimental data at various liquid fill ratios. Although the model correctly predicts the trends associated with the variations in the fill ratio, there are significant differences in the predicted and measured dryout level. Reasons for these differences have been identified and include 1) the insufficient thermal and spatial resolution characteristics of the thermal imaging system utilized in the experimental investigation, 2) omission of the thin film evaporative affects in the analysis, and 3) the inability of the analytical model to account for the progression of the wetted front during a gradual dryout process.

References

[1]Babin, B. R., Peterson, G. P., and Wu, D., "Steady-State Modeling and Testing of a Micro Heat Pipe," *Journal of Heat Transfer*, Vol. 112, No. 3, 1990, pp. 595–601.

[2]Peterson, G. P., "Capillary Priming Characteristics of a High Capacity Dual Passage Heat Pipe," *Chemical Engineering Communications*, Vol. 27, No. 1, 1984, pp. 119–126; also American Society of Mechanical Engineers Paper ASME 82-HT-14, June 1982.

[3]Duncan, A. B., "Experimental and Analytical Investigation of Etched Micro Heat Pipes," Ph.D. Dissertation, Texas A&M Univ., College Station, TX, 1993.

[4]Chi, S. W., *Heat Pipe Theory and Practice*, McGraw-Hill, New York, 1976.

[5]Ivanovskii, M. N., Sorokin, V. P., and Yagodkin, I. V., *The Physical Principles of Heat Pipes*, Oxford Univ. Press, Oxford, England, UK, 1982.

[6]Bankston, C. A., and Smith, H. J., "Vapor Flow in Cylindrical Heat Pipes," *Journal of Heat Transfer*, Vol. 95, 1973, pp. 371–376.

[7]Peterson, G. P., Duncan, A. B., and Weichold, M. H., "Exper-

imental Investigation of Micro Heat Pipes Fabricated in Silicon Wafers," *Journal of Heat Transfer*, Vol. 115, 1993, pp. 751–756.

[8]Ha, J. M., and Peterson, G. P., "Analytical Prediction of the Axial Dryout of an Evaporating Liquid Film in Triangular Microgrooves," *Heat Transfer on the Microscale*, American Society of Mechanical Engineers HTD-Vol. 253, 1993, pp. 53–62.

High-Temperature Performance of an Integral Cesium Reservoir in a Thermionic Converter

K. L. Thayer* and M. L. Ramalingam†
UES, Inc., Dayton, Ohio 45432
and
Timothy J. Young‡
Wright Laboratory,
Wright-Patterson Air Force Base, Ohio 45433

Introduction

THE inclusion of cesium reservoirs in thermionic converters has played a vital role in the production of converters that achieve optimum performance.[1] Cesium vapor in the interelectrode space of a thermionic converter reduces the negative space charge effect on the emitter surface and the work functions of the electrodes due to the adsorption of cesium atoms on their surfaces.[2] The dependence of the cesium vapor pressure p_{cs} on the liquid reservoir temperature T_r is given empirically as[1]

$$p_{cs} = [(2.45 \times 10^8)/\sqrt{T_r}]\exp(-8910/T_r), \text{ Torr} \quad (1)$$

for T_r in Kelvin. Because of the exponential dependence of the cesium pressure on the liquid reservoir temperature, a high degree of temperature control is necessary for the reservoir to maintain a constant cesium pressure. As the liquid reservoir temperature typically ranges from 525 to 625 K (≈0.5 to 6 Torr), and the minimum temperature in the core of the thermionic fuel element (TFE) of the advanced thermionic initiative (ATI) reactor design is approximately 880 K, the liquid reservoir would have to be located external to the core, complicating the overall design of the power system with intricate plumbing and valve arrangements.[3]

Due to the problems cited above, integral, solid sorption reservoirs have been evaluated as an alternative to liquid reservoirs for use in the ATI-TFE design. The potential advantages of such a reservoir are as follows:

1) The reservoir could be designed to operate at a temperature intermediate to the emitter and collector temperatures, thus eliminating the electronic hardware associated with liquid reservoir heaters and temperature controllers.

2) Plumbing and other problems associated with the use of liquid cesium could be eliminated.

3) Optimum cesium pressure could be maintained over a wide range of emitter temperatures due to direct temperature feedback from the converter. Harbaugh and Basiulis[4] investigated the storage characteristics of molybdenum and tungsten reservoirs and tested the performance of these reservoirs in actual converters. They demonstrated optimum converter performance with the reservoirs above 973 K, and also found that the cesium pressure in an adsorption reservoir is less sensitive to changes in reservoir temperature than the cesium pressure in a liquid reservoir. The metal reservoirs were ultimately found to be impractical because of their limited storage capabilities and the variation of vapor pressure, at constant temperature, due to loss of cesium.

Other investigators identified graphite as a potential sorption medium. The intercalation of cesium in graphite forms compounds ranging from C_8Cs to $C_{60}Cs$. Salzano and Aronson[5] characterized these compounds and measured the effect of the graphite reservoir temperature on the cesium vapor pressure. The compounds were found to supply cesium vapor at pressures of 0.5–10 Torr via two-phase equilibrium reactions at temperatures ranging from 700 to 1200 K. The cesium pressure was determined to depend only on the graphite temperature and the reservoir compound. Yates[6] analytically determined the response of a single thermionic cell with an integral reservoir to changes in power input and load resistance and found that sorption reservoirs made from the graphite lamellar compounds provided the best overall response to changes in converter operating conditions.

Thermophysical Characteristics of the Cesium Reservoir

Variation of cesium vapor pressure with reservoir temperature for both liquid and graphite reservoirs suggest, for the reservoirs investigated, that the only applicable cesium-graphite reservoir for direct conductive coupling, without an insulation layer, is the $3C_{24}Cs \rightarrow 2C_{36}Cs + Cs(g)$ equilibrium reaction.[7] The experimental data for the cesium pressure from this graphite reservoir was curve-fitted to generate information for the relationship between pressure and temperature of the graphite reservoir. Once the temperature distribution of the emitter lead region was obtained, the temperature limits of the cesium-graphite equilibrium reaction defined the extreme positions for placement of the graphite reservoir in the lead region. The reservoir could be positioned from 17 to 22 mm from the emitter-lead interface as shown in the schematic in Fig. 1.[3]

Analytical Procedure and Lead Region Thermal Analysis

The nonfueled lead region has approximately 25 mm of emitter substrate to allow a direct conduction path for heat transfer from the hot, fueled region to the cesium-graphite metal-matrix reservoir. The thermionic fuel element pin located at the center of the reactor core receives the maximum thermal input power at steady-state operation and is designated the peak power pin. The average power pin is located between the center of the core and the outer surface.

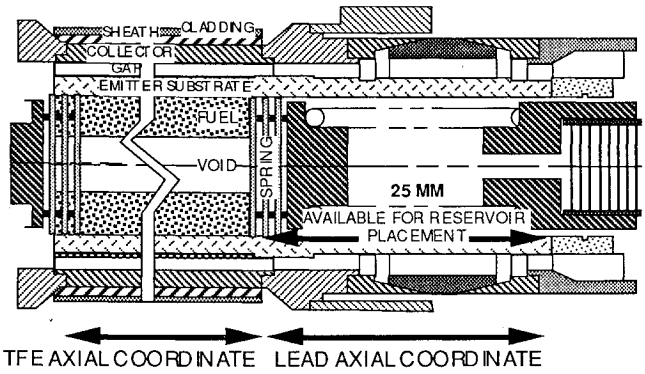

Fig. 1 Schematic of the ATI-TFE design for the location of the reservoir.

Received April 25, 1994; revision received Aug. 25, 1994; accepted for publication Aug. 29, 1994.

*Research Scientist.

†Research Scientist. Associate Fellow AIAA.

‡Engineer, Aerospace Power Division.